Supporting Information

Theoretical calculation and experimental investigation toward the π-conjugated modulation in arylamine derivatives based hole transport materials for perovskite solar cells

Chengyu Wu[a], Ruiqin Wang[a], Jiayi Qi[a], Xin Chen[a], Fei Wu[b,*], Xiaorui Liu[a,*]

[a]Chongqing Key Laboratory of Soft-Matter Material Chemistry and Function Manufacturing, School of Chemistry and Chemical Engineering, Southwest University, Chongqing 400715, P.R. China

[b]Chongqing Key Laboratory for Advanced Materials and Technologies of Clean Energy, School of Materials and Energy, Southwest University, Chongqing 400715, P. R. China

*Corresponding authors

E-mail: feiwu610@swu.edu.cn (F. Wu); liuxiaorui@swu.edu.cn (X. Liu)

S1. Experimental Section

S1.1 Computational Details

The ground-state geometry for investigated molecules CY1 and CY2 were optimized using the B3P86/6-311G(d, p) functional and basis set.[1-6] The energies of all obtained geometries are ensured to be the lowest because the optimized structures do not exhibit imaginary frequency. Energy calculations, including electron affinities, adiabatic ionization potential and reorganization energy of the investigated HTMs were performed using the B3P86/6-311G(d, p) method and basis set. On basis of the ground-state geometry, the optical properties of CY1 and CY2 were calculated by TD-BMK/6-31G(d) functional and basis set in dichloromethane solution with a polarizable continuum model (PCM).[7] In order to calculate the parameter of electronic coupling for HTMs, it was compelled to obtain the dimer structure, which was defined as adjacent segments from the crystal structures of molecules. The crystal structure of the investigated HTMs can be predicted from the polymorph module in Material Studio software.[8] The geometry of the cluster models used in the present study was taken from the B3P86/6-311G(d,p) level. The Deriding force field was used for the prediction.[9] For the investigated molecules, the polymorph calculations are restricted to the six most probable space groups such as $P2_1/c$, $P1$, $P2_12_12_1$, $C2/c$, $P2_1$ and $Pbca$.[10] Then, the crystal structures were sorted according to their total energy. On basis of the crystal structures, to obtain their spatial parameters, a molecule was selected discretionarily as the center of hole transporting, and the adjacent molecules were represented as dimers in different directions which marked as P, T and L. The angle between each jump path and the coordinate axis were labeled θ_P, θ_{Ti} and θ_{Li}. The angle of the final transmission direction relative to the reference axis was defined as Φ. γ was the angle of the hopping pathway relative to the transport plane of the organic crystal molecular stacking layer. To determine the hole transport plane, various planes of each molecule were considered, and the electronic coupling of each dimer in each plane was theoretically calculated. Then, the hole mobility of each plane was calculated using the above formula, and the plane with the largest hole mobility was defined as the final transport plane. Moreover, the calculation details of the hole transfer integral (v), charge-transfer rate (k) and hole mobility (u_h) were reported in previous work.[11-15] The DFT and TD-DFT calculations were carried out by the Gaussian 09 program.[16] The charge transfer integral could be simulated from the PW91/TZP level in ADF program.[17, 18]

S1.2 Synthesis of HTMs

N3,N3,N6,N6-tetrakis(4-methoxyphenyl)-9-(4-(naphthalen-2-yl)phenyl)-9H-carbazole-3,6-diamine (**CY1**): The naphthalen-2-ylboronic acid (85.955 mg, 0.50 mmol) and the 9-(4-bromophenyl)-N3,N3,N6,N6-tetrakis (4-methoxyphenyl)-9H-carbazole-3,6-diamine (310.688 mg, 0.40 mmol) were accurately weighed and putted into a round-bottomed flask (250 mL). The connected instrument was replaced by vacuum extraction for three times to fill the device with argon gas. Under argon atmosphere, the catalyst $Pd(PPh_3)_4$ (0.05 mmol, 57.8 mg) was transferred to the flask. Pre-deoxygenated toluene (15 mL) solution and K_2CO_3 (2 M 2.5 mL) solution were injected into the flask. The reaction was reflux at 110 ℃ for 24 h. After monitoring the reaction, the system was cooled to room temperature, extracted with dichloromethane (DCM), and dried with anhydrous Na_2SO_4 for 3 h. After vacuum extraction and filtration, the most of the solvent was removed using a rotary evaporator. Finally, the crude product was purified by column chromatography on silica gel (eluent: EA:PE = 1:4) to obtain white solid powder (270.6 mg, yield: 82.16%). ^{1}H NMR (600 MHz, DMSO-d6) δ 8.35 (s, 1H), 8.09 (d, J = 8.5 Hz, 2H), 8.05 (t, J = 9.4 Hz, 2H), 7.97 (t, J = 9.9 Hz, 2H), 7.73 (d, J = 9.4 Hz, 4H), 7.60 – 7.53 (m, 2H), 7.38 (d, J = 8.7 Hz, 2H), 7.10 (d, J = 8.8 Hz, 2H), 6.88 (d, J = 9.0 Hz, 8H), 6.82 (d, J = 9.0 Hz, 8H). ^{13}C NMR (151 MHz, DMSO-d6) δ 154.81, 142.41, 141.91, 137.56, 132.40, 128.40, 127.86, 127.02, 124.97, 124.55, 124.45, 124.06, 116.98, 115.17, 111.40, 55.65, 40.03.

N3,N3,N6,N6-tetrakis(4-methoxyphenyl)-9-(4-(pyren-1-yl)phenyl)-9H-carbazole-3,6-diamine (**CY2**): The pyren-1-ylboronic acid (123.035 mg, 0.50 mmol) and the 9-(4-bromophenyl)-N3,N3,N6,N6-tetrakis (4-methoxyphenyl)-9H-carbazole-3,6-diamine (310.688 mg, 0.40 mmol) were accurately weighed and putted into a round-bottomed flask (250 mL). The connected instrument was replaced by vacuum extraction for three times to fill the device with argon gas. Under argon atmosphere, the catalyst $Pd(PPh_3)_4$ (0.05 mmol, 57.8 mg) was transferred to the flask. Pre- deoxygenated toluene (15 mL) solution and K_2CO_3 (2 M 2.5 mL) solution were injected into the flask. The reaction was reflux at 110 ℃ for 24 h. After monitoring the reaction, the system was cooled to room temperature, extracted with dichloromethane (DCM), and dried with anhydrous Na_2SO_4 for 3 h. After vacuum extraction and filtration, the most of the solvent was removed using a rotary evaporator. Finally, the crude product was purified by column chromatography on silica gel

(eluent: EA:PE = 1:5) to obtain white solid powder (287.6 mg, yield: 80.14%). ^{1}H NMR (600 MHz, DMSO-d6) δ 8.42 (d, J = 7.9 Hz, 1H), 8.34 (dd, J = 17.7, 7.6 Hz, 2H), 8.25 (d, J = 13.5 Hz, 4H), 8.17 – 8.09 (m, 2H), 7.90 (d, J = 8.0 Hz, 2H), 7.83 (d, J = 7.5 Hz, 2H), 7.75 (s, 2H), 7.51 (d, J = 8.8 Hz, 2H), 7.14 (d, J = 8.8 Hz, 2H), 6.90 (d, J = 9.1 Hz, 8H), 6.83 (d, J = 9.4 Hz, 8H), 3.70 (s, 12H). ^{13}C NMR (151 MHz, DMSO-d6) δ 154.82, 142.41, 141.86, 137.53, 129.12, 129.02, 128.78, 128.01, 127.47, 126.99, 125.92, 125.44, 124.97, 124.45, 123.99, 116.98, 115.17, 111.29, 55.65, 40.03.

S1.3 Device Fabrication

To measure the photovoltaic performance of PSCs, a structure of FTO/TiO_2/ $Cs_{0.05}FA_{0.85}MA_{0.10}Pb(I_{0.97}Br_{0.03})_3$/HTMs/Ag were fabricated. The patterned FTO glass (Advanced Election Technology CQ,. Ltd.) were cleaned sequentially washed with detergent, deionized water, acetone, isopropanol in an ultrasonic bath and then dried by flowing air. The preparation method for compact layer of TiO_2 was reported in our previous work.[19, 20] Then the FTO substrates were transferred into N_2 glovebox. The preparation of perovskite film was from the work of Grätzel.[21] Perovskite precursor solution was prepared by dissolving a mixture of PbI_2 (1.61 mmol, 742.0 mg), FAI (1.31 mmol, 224.4 mg), MABr (0.15 mmol, 16.2 mg), and CsI (0.08 mmol, 19.8 mg) in 1 mL of mixed solution of DMF and DMSO [DMF (v):DMSO (v) = 4:1]. The mixed perovskite precursor is stirred for 12 h in N_2 glovebox. PbI_2, FAI, $PbBr_2$, MABr and CsI were purchased from the commercial vendors of Advanced Election Technology CQ. Ltd. Anhydrous DMSO (99.8%) and DMF (99.8%) were purchased from Sigma Aldrich. The perovskite solution was spin-coated onto the FTO/TiO_2 substrate in a two-step program at 2000 and 6000 rpm for 10 and 30 s, respectively. During the second step, 100 μL of anhydrous chlorobenzene (99.8%, Macklin Biochemical Technology Co., Ltd., Shanghai) was dropped on the spinning substrate at 15 s after the start-up. In order to drive off solvent and form the perovskite phase, the perovskite layer was annealed on a hot plate at 120 °C for 20 min. The HTM solution was each prepared by dissolving Spiro-OMeTAD (72.3 mg mL^{-1}) in 1 mL chlorobenzene, 28.8 mL tert-butylpyridine (TBP) solution and 17.5 mL lithium bis(trifluoro methylsulfonyl) imide (Li-TFSI)/acetonitrile (520 mg mL^{-1}). Spiro-OMeTAD (99.5%) was purchased from Advanced Election Technology CQ., Ltd. Lithiumbis-(trifluoromethylsulfonyl)imide (LiTFSI, 99%) and 4-(tert-Butyl)pyridine (*t*BP, 99%) were purchased from Bide Pharmatech CO., Ltd.. CY1 and CY2 were dissolved in chlorobenzene in a

concentration of 40 mg mL^{-1}, with 28.7 μL TBP and 17.5 μL Li-TFSI as dopants. The devices were pumped to lower than 10^{-5} Pa for the deposition of 80 nm silver. The active area of our device is 0.06 cm^2.

S1.4 Hole Mobility Measurements

Hole-only devices were fabricated with the structure ITO/PEDOT:PSS/HTM/MoO_3/Ag. PEDOT:PSS (Heraeus, Clevios PVP Al 4083) were purchased from Advanced Election Technology CQ., Ltd. MoO_3 (99.99%) was purchased from Xi'an Polymer Light Technology CO., Ltd., China. The dark *J–V* characteristics of hole-only devices were measured under N_2 atmosphere inside a glove box. PEDOT:PSS was deposited on the ITO substrate at 5000 rpm for 30 s, followed by annealing at 120 ºC for 30 min. The conditions of spin coating HTMs are consistent with the device fabrication. Mobility is extracted by fitting the current density-voltage curves using space charge limited current (SCLC). Fitting the results to a space charge limited form, based on the following equation $J = 9\varepsilon_\theta\varepsilon_\gamma\mu_h V^2/8L^3$. [22] J is the current density, L is the film thickness of the active layer, μ_h is the hole mobility, ε_γ is the relative dielectric constant of the transport medium ($\varepsilon_\gamma = 3$ for organic materials), ε_θ is the permittivity of free space (8.85×10^{-12} F m^{-1}), V is the internal voltage of the device.

S1.5 Measurements

The nuclear magnetic resonance (NMR) spectra were obtained from a BRUKER AVANCE Ⅲ 600 MHz NMR Instrument (in DMSO-d_6, 99.9%, Beijing Hwrkchemical Co., Ltd.). Mass spectra were collected on a Bruker impact II high-resolution mass spectrometer. UV-vis absorption spectra were measured on a Shimadzu UV-2450 absorption spectrophotometer. Absorption spectra in solution were recorded in dichloromethane solution with a HTM concentration of 10^{-5} M. Cyclic voltammetry studies were conducted using a CHI660E system in a typical three-electrode cell with a glass carbon working electrode, a platinum wire counter electrode, and a silver/silver chloride (Ag/AgCl) reference electrode. All electrochemical experiments were carried out under a nitrogen atmosphere at room temperature in an electrolyte solution of 0.1 M tetrabutylammonium hexa-fluorophosphate (Bu_4NPF_6) in dichloromethane at a sweeping rate of 50 mV s^{-1}. The potential of Ag/AgCl reference electrode was internally calibrated by using the ferrocene/ferrocenium redox

couple (Fc/Fc^+). According to the onset oxidation potential of the CV measurements, the highest occupied molecular orbital (HOMO) was estimated based on the vacuum energy level of ferrocene (5.1 eV): HOMO = – (E_{onset} – $E_{Fc/Fc+}$) – 5.1 eV. The current–voltage (*J–V*) curves were measured under 100 mW cm^{-2} (AM 1.5 G) simulated sunlight using Keithley 2400 in conjunction with a Newport solar simulator (94043A). Film thickness of hole transport layer and perovskite layer were measured by Surfcorder ET200A, Kosaka Laboratory Ltd. Using atomic force microscopy (AFM) to characterize the morphology, the model is CSPM5500A.

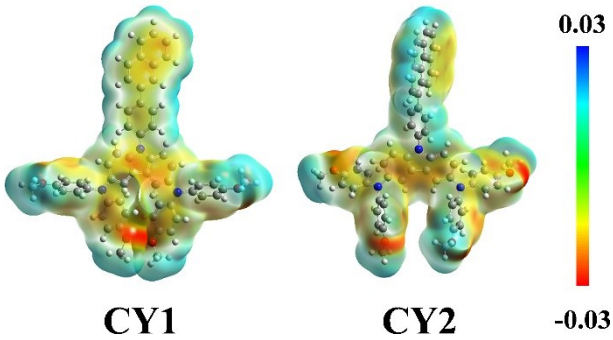

Fig. S1 Electrostatic surface potential (ESP) of CY1 and CY2.

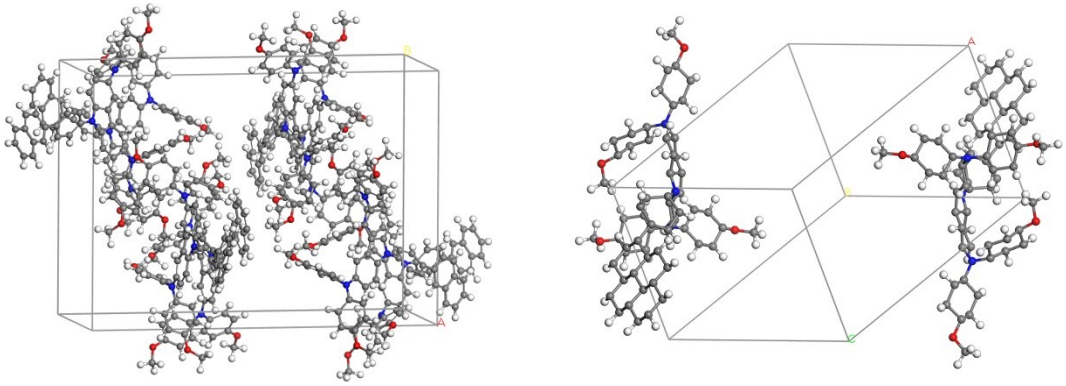

CY1 **CY2**

Fig. S2 Simulated crystal structures with the lowest total energies of CY1 and CY2.

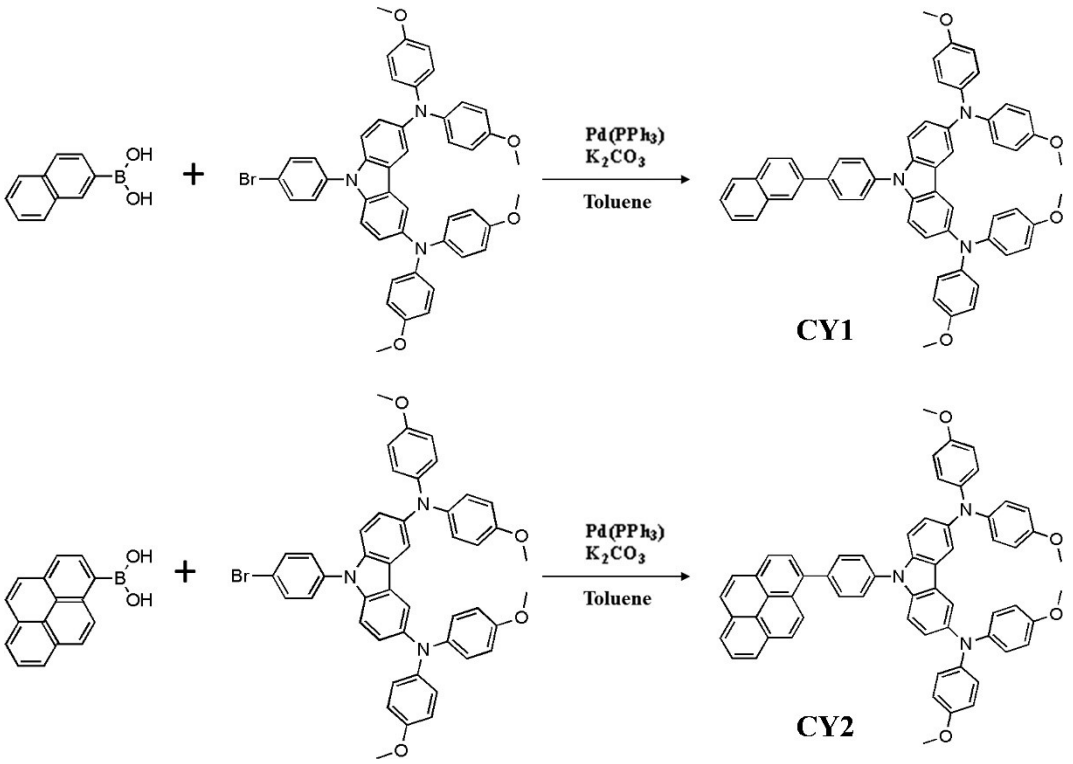

Fig. S3 Synthesis route of CY1 and CY2.

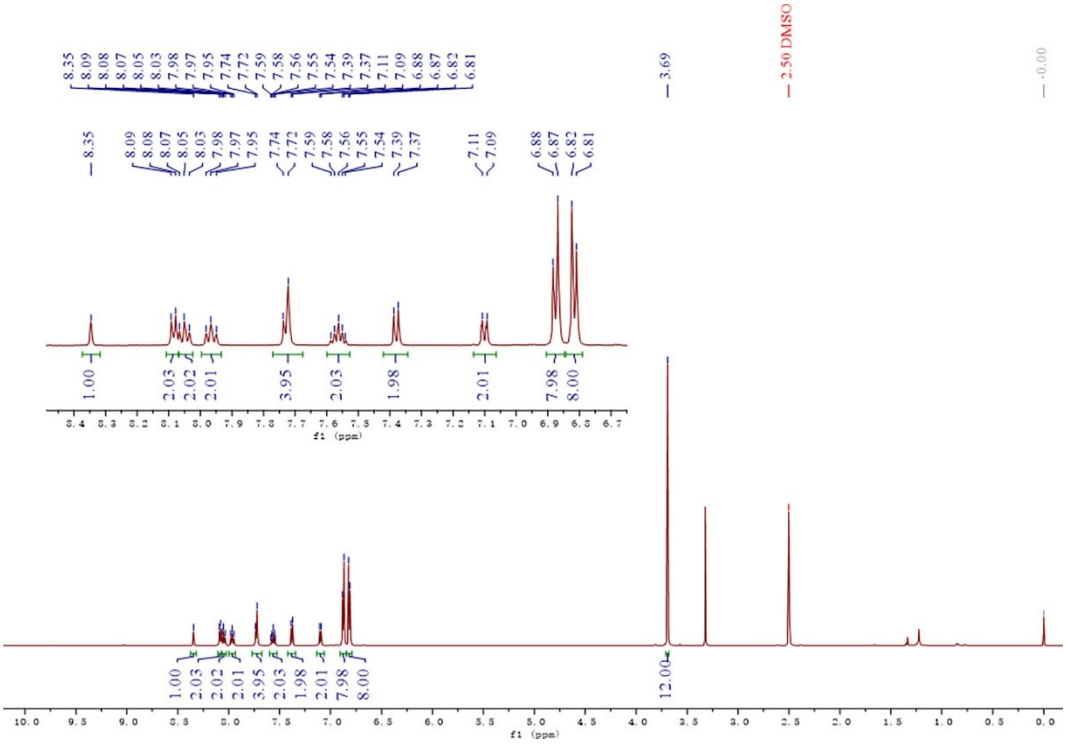

Fig. S4 ^{1}H NMR spectrum of CY1 in DMSO.

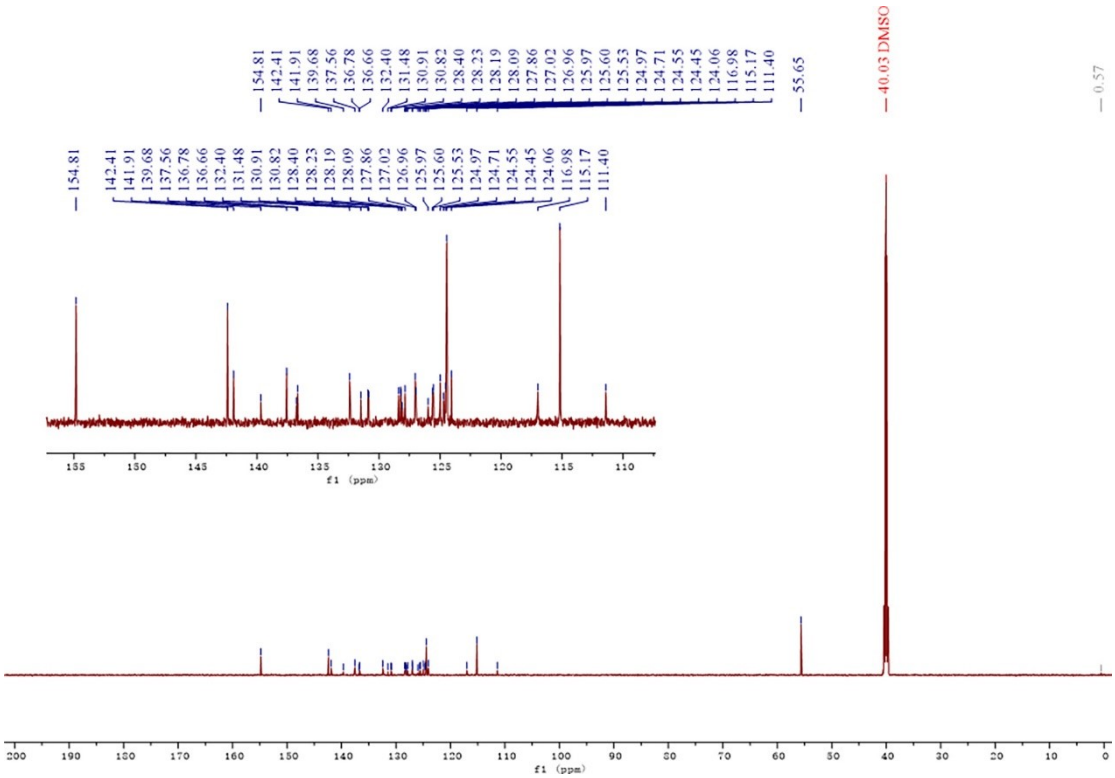

Fig. S5 ^{13}C NMR spectrum of CY1 in DMSO.

Mass Spectrum SmartFormula Report

Analysis Info

Analysis Name C:\Users\Karry\Desktop
Method DirectInfusion - MS - positive.m
Sample Name
Comment

Acquisition D 2023/3/2 12:02:45

Operator Demo User
Instrumen impact II 1825265.10221

Acquisition Paramet

Source Type	ESI	Ion Polarity	Positive	Set Nebulizer	0.4 Bar
Focus	Active	Set Capillary	4500 V	Set Dry Heater	180 °C
Scan Begin	50 m/z	Set End Plate Offset	-500 V	Set Dry Gas	0.8 l/min
Scan End	1300 m/z	Set Charging Voltage	2000 V	Set Divert Valve	Source
		Set Corona	0 nA	Set APCI Heater	0 °C

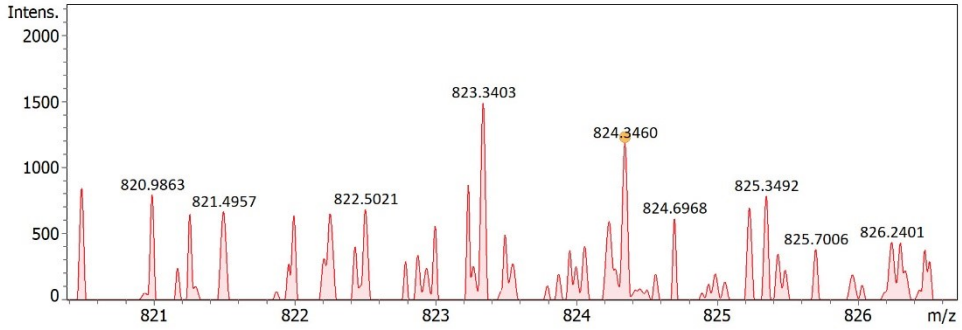

Meas. m/z	#	Ion Formula	m/z	err [ppm]	mSigma	# mSigma	Score	rdb	e¡¥	Conf	N-Rule
824.3460	1	C56H46N3O4	824.3483	2.8	103.7	1	100.00	36.0	even		ok

Fig. S6 High resolution mass spectrometry of CY1.

MASS SPECTROMETRY REPORT

Sample No.	Formula (M)	Measured m/z	Calc. m/z	Diff (ppm)
CY1	$C_{56}H_{45}N_3O_4$	823.3403	823.3410	-0.85

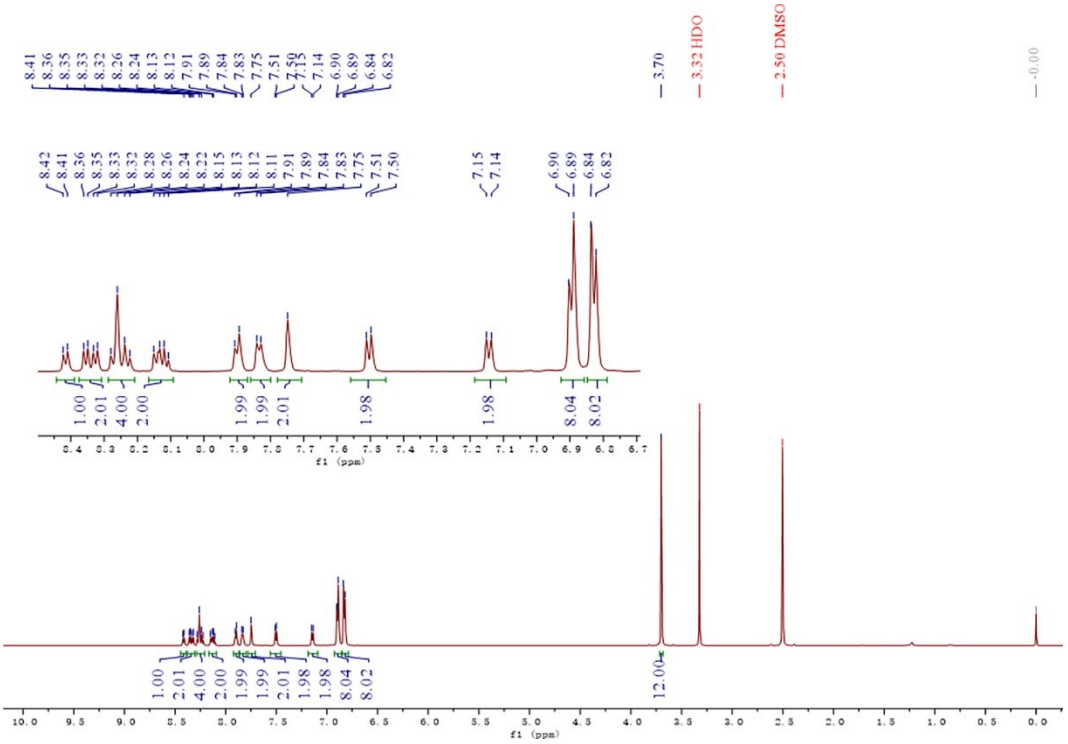

Fig. S7 ^{1}H NMR spectrum of CY2 in DMSO.

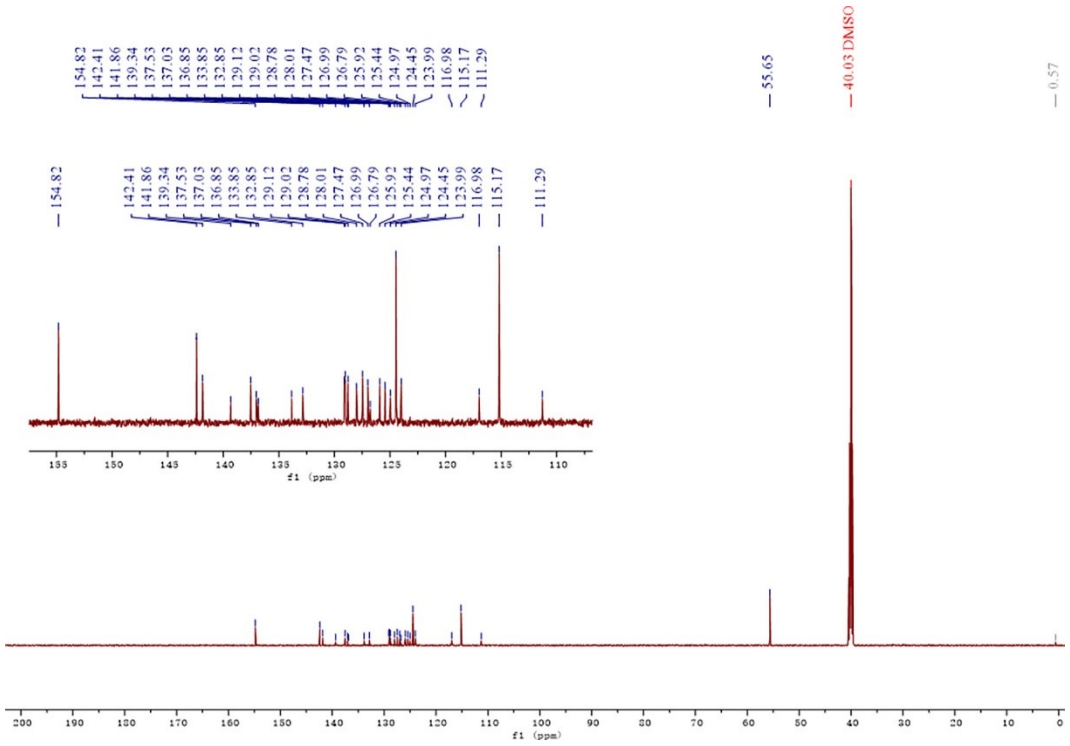

Fig. S8 ^{13}C NMR spectrum of CY2 in DMSO.

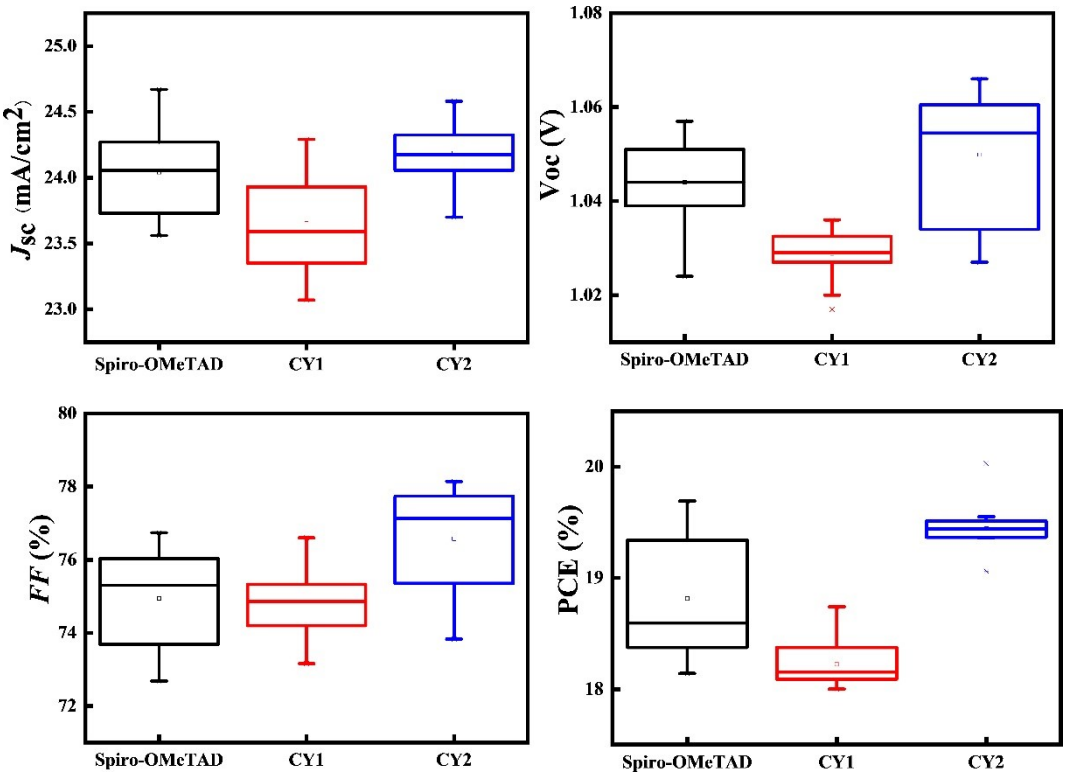

Fig. S9 Box charts of the photovoltaic parameters of HTMs.

Table S1. Predicted crystal data of CY1 and CY2.

Compounds	Space group	a(Å)	b(Å)	c(Å)	α(°)	β(°)	γ(°)
CY1	*Pbca*	21.905196	14.085505	30.282169	90.000	90.000	90.000
CY2	*P1*	11.713397	15.313071	18.632639	70.87553	106.58209	71.59114

Table S2. Summary of hysteresis index (HI) and device performance of perovskite solar cell adopting CY1 and CY2 at forward and reverse voltage scans.

HTM		J_{sc} [mA cm^2]	V_{oc} [V]	*FF* [%]	PCE [%]	HI[a] [%]
Spiro-OMeTAD	forward	24.28	1.057	76.74	19.69	4.16
	reverse	24.19	1.054	74.00	18.87	
CY1	forward	24.06	1.028	75.76	18.74	3.36
	reverse	23.90	1.034	73.29	18.11	
CY2	forward	24.36	1.057	77.80	20.03	2.74
	reverse	24.23	1.063	75.64	19.48	

[a]HI = $[(PCE_{forward} - PCE_{reverse})/PCE_{forward}] \times 100\%$

References

1. S. Ghosh, P. Verma, C. J. Cramer, L. Gagliardi and D. G. Truhlar, *Chem. Rev.* 2018, **118**, 7249-7292.
2. F. Tran, J. Doumont, L. Kalantari, A. W. Huran, M. A. L. Marques and P. Blaha, *J. Appl. Phys.* 2019, **126**, 110902.
3. A. D. Becke, *J. Chem. Phys.* 1993, **98**, 5648-5652.
4. A. D. Becke, *J. Chem. Phys.* 1998, **109**, 2092-2098.
5. P. Borlido, T. Aull, A. W. Huran, F. Tran, M. A. L. Marques and S. Botti, *J. Chem. Theory Comput.* 2019, **15**, 5069-5079.
6. P. Verma and D. G. Truhlar, *Trends in Chemistry* 2020, **2**, 302-318.
7. J. Tomasi, B. Mennucci and R. Cammi, *Chem. Rev.* 2005, **105**, 2999-3094.
8. K. Senthilkumar, F. Grozema, F. Bickelhaupt and L. Siebbeles, *J. Chem. Phys.* 2003, **119**, 9809-9817.
9. R. F. Jin and Y. F. Chang, *Phys. Chem. Chem. Phys.* 2015, **17**, 2094-2103.
10. W.-J. Chi and Z.-S. Li, *Phys. Chem. Chem. Phys.* 2015, **17**, 5991-5998.
11. H. Liu, H. Sun, Q. Chen, F. Wu and X. Liu, *Appl. Surf. Sci.* 2022, **604**, 154603.
12. Q. Chen, H. Liu, R. Wang, C. Wu, F. Wu, X. Liu and X. Liu, *Dyes Pigm*. 2022, **206**, 110604.
13. J. Yang, W. Hu, j. Yi, J. Zhao and L. Xu, *Dye Pigm*. 2022, **204**, 110370.
14. Z.-Z. Sun, J. Yang, W.-L. Ding, J.-L. Liu and X.-L. Xu, *J. Phys. Chem. C*. 2022, **126**, 11529-11536.
15. T. Liu, K. S. Sun, R. X. He, Z. M. Zhang, W. Shen and M. Li, *J. Phys. Chem. C*. 2018, **122**, 8804-8813.
16. M. J. Frisch, G. W. Trucks, H. B. Schlegel, G. E. Scuseria, M. A. Robb, J. R. Cheeseman, G. Scalmani, V. Barone, G. A. Petersson, H. Nakatsuji, X. Li, M. Caricato, A. Marenich, J. Bloino, B. G. Janesko, R. Gomperts, B. Mennucci, H. P. Hratchian, J. V. Ortiz, A. F. Izmaylov, J. L. Sonnenberg, D. Williams-Young, F. Ding, F. Lipparini, F. Egidi, J. Goings, B. Peng, A. Petrone, T. Henderson, D. Ranasinghe, V. G. Zakrzewski, J. Gao, N. Rega, G. Zheng, W. Liang, M. Hada, M. Ehara, K. Toyota, R. Fukuda, J. Hasegawa, M. Ishida, T. Nakajima, Y. Honda, O. Kitao, H. Nakai, T. Vreven, K. Throssell, J. A. Montgomery, Jr., J. E. Peralta, F. Ogliaro, M. Bearpark, J. J. Heyd, E. Brothers, K. N. Kudin, V. N. Staroverov, T. Keith, R. Kobayashi, J. Normand, K. Raghavachari, A. Rendell, J. C. Burant, S. S. Iyengar, J. Tomasi, M. Cossi, J. M. Millam, M. Klene, C. Adamo, R. Cammi, J. W. Ochterski, R. L. Martin, K. Morokuma, O. Farkas, J. B. Foresman, and D. J. Fox. Gaussian 09, revision A.01. Wallingford, CT: Gaussian, Inc. 2009.
17. G. te Velde, F. M. Bickelhaupt, E. J. Baerends, C. Fonseca Guerra, S. J. A. van Gisbergen, J. G. Snijders and T. Ziegler, *J. Comput. Chem*. 2001, **22**, 931-967.
18. C. Fonseca Guerra, J. G. Snijders, G. te Velde and E. J. Baerends, *Theor Chem Acc*. 1998, **99**, 391-403.
19. R. Q. Wang, C. Y. Wu, J. Y. Qi, W. Shen, F. Wu, M. Li, R. X. He and X. R. Liu, *Adv. Funct. Mater.* 2023, **33**, 2213843.
20. R. Q. Wang, R. Wang, X. Chen, C. Y. Wu, F. Wu and X. R. Liu, *Dyes Pigm.* 2023, **212**, 111097.
21. H. Zhu, Y. Liu, F. T. Eickemeyer, L. Pan, D. Ren, M. A. Ruiz-Preciado, B. Carlsen, B. Yang, X. Dong, Z. Wang, H. Liu, S. Wang, S. M. Zakeeruddin, A. Hagfeldt, M. I. Dar, X. Li and M. Gratzel, *Adv. Mater.* 2020, **32**, e1907757.
22. V. D. Mihailetchi, J. Wildeman and P. W. Blom, *Phys Rev Lett*. 2005, **94**, 126602.